Available online at www.sciencedirect.com
SCIENCE DIRECT
Journal of Catalysis 238 (2006) 142–152
JOURNAL OF CATALYSIS
www.elsevier.com/locate/jcat

Combinatorial discovery of new autoreduction catalysts for the CO_2 reforming of methane

Do Kyoung Kim, Wilhelm F. Maier *

Lehrstuhl für Technische Chemie, Universität des Saarlandes, Gebäude C 4.2, 66123 Saarbrücken, Germany

Received 7 October 2005; revised 1 December 2005; accepted 3 December 2005

Available online 9 January 2006

Abstract

High-throughput synthesis and screening techniques were used in the search for and optimization of new autoreduction catalysts for the CO_2 reforming of methane. Diverse libraries had been synthesized via three different modified sol–gel methods using a synthesis robot and library design software. The catalyst libraries were screened for catalytic activity and stability in a simple high-throughput reactor system at 600 °C connected to a micro-gas chromatograph for product analysis. During generations 1 and 2, more than 5000 highly diverse mixed oxides were tested for potential catalytic activity. $Ni_{10}Ce_{90}O_x$ demonstrated effective activity and stability among nonprecious metal catalysts without a prereduction step. In a conventional study, two advantages (i.e., rapid startup operation and high coking resistance) of $Ni_{10}Ce_{90}O_x$ were noted relative to the well-known Ni/Al_2O_3, but deactivation was recognized. To reduce deactivation of $Ni_{10}Ce_{90}O_x$, catalyst libraries with additional dopants were prepared and examined during generations 3 and 4. Among these, $(Al_5, Al_{15}, Zr_{15})Ni_{10}Ce_{90-y}O_x$, in which metal nitrate was used as a dopant precursor, and $(Al_{15}, Zr_5, Zr_{15})Ni_{10}Ce_{90-y}O_x$, in which metal alkoxide was used, exhibited comparable activity and strongly reduced deactivation compared with $Ni_{10}Ce_{90}O_x$. Good performance of the best new catalysts, particularly $Al_{15}Ni_{10}Ce_{75}O_x$, in which aluminium alkoxide was used as a dopant precursor, and $Zr_{15}Ni_{10}Ce_{75}O_x$, in which zirconium dinitrate oxide was used, was found in high-throughput studies and confirmed in conventional experiments.

Keywords: Methane reforming; CO_2; Autoreduction; Ceria; Nickel catalysts; Combinatorial chemistry; High-throughput experimentation (HTE); Heterogeneous catalysis; Sol–gel; Amorphous mixed oxides

1. Introduction

Concern about the high dependence of our economies on crude oil has generated increasing interest in the use of alternative fuel sources. One of the most attractive renewable energy resources is biogas, which is composed of 50–60% CH_4, 40–50% CO_2, and moisture [1]. Use of the "greenhouse" gases CH_4 and CO_2 with important environmental implications is receiving increasing attention [2]. Principally, CH_4 and CO_2 can be used directly as sources for the CO_2 reforming of methane to produce syngas [3]. Syngas is a valuable feedstock for the production of higher hydrocarbons (Fisher–Tropsch synthesis) or methanol. In addition, in conjunction with the water–gas shift (WGS) reaction, it may be applied to produce hydrogen, the main feed gas for fuel cell applications, and ammonia synthesis. When distributed in reduced form on suitable supports, group VIII metals (including Ni, Ru, Rh, Pd, Ir, and Pt) become effective catalysts for the CO_2 reforming of methane [3–7]. For economic reasons (low cost and high availability), most state-of-the-art technologies are based on nickel catalysts. Nickel catalysts are susceptible to a severe, inactive carbon deposition leading to reactor plugging. Besides catalyst activity and stability, rapid startup operation with no prereduction step is a requirement for such a reforming catalyst for applications in portable and small-scale stationary fuel cells. The development of reforming catalysts, which do not require in situ preconditioning, has received industrial attention [8], although only few reports are available for such catalysts [9,10]. In both industrial and academic studies, precious metal-based catalysts are dominating the published investigations. Therefore, new noble metal-free catalysts of high catalytic activity, lack of coking,

* Corresponding author.
E-mail address: w.f.maier@mx.uni-saarland.de (W.F. Maier).

0021-9517/$ – see front matter
doi:10.1016/j.jcat.2005.12.001

and rapid startup operation with no prereduction step are of great interest in the CO_2 reforming of methane.

The development and application of high-throughput methods for the rapid discovery and optimization of solid-state catalysts has led to promising results in the last few years [11–15]. Evolutionary algorithms, which control the sequence of generations for catalyst or material development without requiring choices and decisions by the chemist, have been successfully applied to the optimization of heterogeneous catalysts [16,17] and phosphorous materials [18] within limited parameter spaces. Because we started here with a highly diverse primary screening space, such algorithms were not applied.

In our research group, high-throughput synthesis and screening techniques have successfully been used in the search for and optimization of new catalysts [19–24]. The Plattenbau program was used for the experimental design and generation of pipetting lists for the synthesis robots [25]. The catalysts were synthesized in vials with the aid of a pipetting robot and calcined after gelation. The mixed-oxide powders formed were transferred manually to the 207 wells of a library plate. The catalytic performance of each material on the library can be tested by high-throughput technologies, such as emissivity-corrected infrared (IR) thermography [22–24] and spatially resolved mass spectrometry [19,20] or gas chromatography [21]. The process of the high-throughput experiments was controlled by the software TestRig software [20]. These technologies have been adopted in the search for new reforming catalysts.

In the present study, new autoreduction catalysts for the CO_2 reforming of methane were screened in a high-throughput gas chromatography (GC) screening setup, followed by a scale-up of the synthesis and confirmation of promising results under conventional gas-phase reaction conditions.

2. Experimental

2.1. High-throughput experiment

Studying CO_2-reforming of methane by high-throughput methods is not a trivial task. Because the reaction is an equilibrium reaction carried out at high temperatures, IR thermography cannot be used. Suitable methods include spatially resolved mass spectrometry or GC. It is well known that heterogeneous catalysts are very sensitive to preparation conditions. For example, preparation of 100 catalysts of the identical chemical composition by different synthesis procedures and different pre- or after treatments will result in 100 materials of different catalytic activity, ranging most likely from inactive to highly active. In high-throughput searches for new catalyst compositions it is essential, that catalyst preparation is carried out under identical conditions. Variations in chemical composition or doping with a wide range of elements must be carried out with a common synthesis procedure that is very tolerant to such compositional changes. Therefore, many conventional catalyst preparations are not useful in such a search. We have developed highly tolerant synthesis recipes, which allow the broad screening of elemental compositions based on sol–gel procedures [23,24,26]. These recipes have been used to prepare a large variety of mixed oxides, which can then be tested for catalytic performance.

Our general strategy for high-throughput screening involves not only the creation of a library of spatially separated catalysts, but also the evaluation of the library through catalyst activity and stability testing. Typically, up to 207 catalyst compositions in a library were prepared and measured in each experiment.

2.2. High-throughput syntheses of catalyst libraries

The automated synthesis of catalysts was done using a commercial pipetting robot (Lissy, Zinsser Analytic). In the procedure, 1 M matrix and 0.1 M dopant stock solutions were positioned in 10 ml vials and used to formulate the final reaction mixture by transferring the aliquots of each stock solution into 2-ml vials, positioned in racks of 50 vials. Alcoholic solutions of metal nitrates (Ag, Al_N, Ba, Ca, Cd, Ce, Co, Cr, Cs, Cu, Dy, Er, Eu, Fe, Ga, Gd, Ho, In, K, La, Li, Lu, Mg, Mn, Na, Nd, Ni, Pb, Pr, Sc, Sm, Sr, Tb, Tm, Y, and Yb), alkoxides (Al_A, Bi, Ge, Mo, Nb, Pd, Rb, Si, Sn, Ta, Ti, V, W, and Zr_A), chlorides (Hf, Ir, Re, Rh, Ru, Sb, Sn, and Te), bromides (Au and Pt), dinitrate oxide (Zr_N), acid (B), and oxide (Se) were used as standard dopant precursors. Subscripts were used to distinguish dopant elements based on the different kinds of precursors (i.e., "N" for metal nitrate and "A" for metal alkoxide). Because all catalyst materials were mixed oxides, and the oxidation state of the oxides was not determined and was subject to experimental conditions, in what follows the materials are identified only by the metal ions and atomic % given as a subscript; for example, $Nb_{37}Cs_{63}$ means a mixed oxide comprising 37% of Nb and 63% of Cs oxides.

The synthesis of the combinatorial catalyst libraries was accelerated using the Plattenbau library design software [25]. This software calculates, based on a parameterized recipe, the volumes of the different solutions of starting materials, as required for the preparation of the individual samples. It also generates an optimized pipetting list, which can be transferred directly to the pipetting robot.

Three different kinds of modified sol–gel procedures were applied to prepare libraries depending on the matrix metal precursor used (i.e., method 1 for alkoxide, method 2 for propionate, and method 3 for nitrate) as follows. The prepared samples are identified by the central elements with the expected mol% from the composition of the starting sol given in subscripts. The total molar amount of dopant and matrix was set as 200 μmol per sample.

Method 1. This method followed procedures similar to those described in detail previously [26]. Briefly, the molar ratio of dopant:matrix:water:acid (nitric acid for $E_xZr_{20}Al_{80-x}$ or acetic acid for M_3N_{97}):complexing agent (4-hydroxy-4-methyl-pentanone):alcohol (iso-propanol) was x:$(100-x)$:100:6:300:6500. The preparation of $Ni_5Zr_{20}Al_{75}$, for example, was carried out by pipetting the following volumes of single solutions in the following sequence: complexing agent (74.1 μl, 600 μmol), 1 M $Zr[O(CH_2)_2CH_3]_4$ in isopropanol (40.0 μl, 40 μmol), 1 M $Al[C_2H_5CH(CH_3)O]_3$ in isopropanol (150.0 μl,

150 μmol), 0.1 M $Ni(NO_3)_2{\cdot}6H_2O$ in isopropanol (100.0 μl, 10 μmol), isopropanol (705.4 μl, 9213 μmol), water (3.6 μl, 200 μmol), and nitric acid (0.5 μl, 12 μmol). The $E_xZr_{20}Al_{80-x}$ with 59 dopant (E) of three different loading level ($x = 1$, 5, 10) and the M_3N_{97} (N = Cu, Fe, Nb, Sn, Ta, V) with 55 dopant (M) were set by this method.

Method 2. This method followed procedures similar to those described in detail previously [23]. In brief, the molar ratio of dopant:matrix:complexing agent (4-hydroxy-4-methyl-pentanone):alcohol (ethanol) was 3:97:300:2542. For example, Ni_3Co_{97} was prepared by pipetting the following volumes of single solutions in sequence: 1 M cobalt propionate in ethanol mixed with ethanol and complexing agent (0.34 M, 564.6 μl, 194 μmol) and 0.1 M $Ni(NO_3)_2{\cdot}6H_2O$ in methanol (60.0 μl, 6 μmol). The M_3P_{97} (P = Co, Mn, Ni) with 55 dopant (M) was prepared by this method.

Method 3. The molar ratio of dopant (0.1 M solution in alcohol):matrix (1 M nitrate solution in methanol):complexing agent (4-hydroxy-4-methyl-pentanone):acid (propionic acid) was 3:97:300:2. The preparation of Ni_3Ce_{97} was performed by pipetting the following volumes of single solutions in sequence: 1 M $Ce(NO_3)_3{\cdot}6H_2O$ in methanol (194.0 μl, 194 μmol), 0.1 M $Ni(NO_3)_2{\cdot}6H_2O$ in methanol (60.0 μl, 6 μmol), and complexing agent mixed with propionic acid (8.06 M, 74.5 μl, 600 μmol). The M_3Q_{97} (Q = Ce, Cr, Ga, In, Zn) with 55 dopant (M) was set by this method.

After the pipetting process of an entire rack was completed, this rack was covered and placed on an orbital shaker (Titramax 100; Heidolph) for 3 h. After removing the lid, the rack was dried for 5 days at 40 °C to allow gel formation and catalyst drying. All samples were calcined in an oven at 65 °C for 5 h (at a heating rate of 0.2 °C min^{-1}) and at 250 °C for 5 h (at a heating rate of 0.2 °C min^{-1}). The catalyst powders obtained were ground in HPLC flasks and manually transferred into 207 hexagonally positioned wells (∅ 3.5 mm) in a stainless steel library plate (∅ 99 mm), as shown in Fig. 1. Some wells were left empty for background, and one well was filled with a reference catalyst. The activity of each well was obtained from the amount of CO produced on the catalyst and represented relative to the activity of the reference catalyst. Therefore, the relative activity (%) of each sample was defined as [(the amount of CO produced on a sample)/(the amount of CO produced on the reference catalyst)×100]. For comparison, 10 mol% Ni catalyst supported on commercial γ-Al_2O_3 (Johnson Matthey; $S_{BET} = 255\ m^2\ g^{-1}$), referred to as Ni/$Al_2O_3$, was prepared using the wet impregnation method in a conventional manner and was filled in a well. The library was calcined again in an oven, heated to 700 °C at a heating rate of 2 °C min^{-1}, and kept there for 2 h.

Fig. 1. Image of a stainless-steel library plate (∅ 99 mm) with 207 hexagonally positioned wells (∅ 3.5 mm), filled with catalysts.

2.3. High-throughput testing of catalyst libraries

The open-well, high-throughput reactor system used in the present study has been described previously [19–21]. Briefly, the catalyst library is placed in a special reactor with a heating system and insulation (see Fig. 2). On top of the library, a 15-mm-thick ceramic mask with drillings provides additional reaction volume on the top of each well and insulates the library plate to improve the constant of the reaction temperature on the catalyst surface. A capillary bundle containing both the educt gas supply and the product gas sampling system is inserted sequentially into each well of the library plate. The position of the capillary bundle is fixed while the complete reactor is moved. The movement of the reactor is provided by an xyz-stage.

Our original reactor system was not reliable at the temperature range of 600–800 °C needed for this investigation. To improve the thermal stability of the reactor at high temperature, the modifications of the previous reactor involved a change in the reactor parts materials. Whereas the original reactor was constructed from V4A-steel, high-heat-resistant steel was used for all parts of the new reactor. In addition, a thicker insulating mantle for high temperatures was wrapped around the reactor. The insulating mask was made from MACOR (thickness 12.5 mm) and was in direct contact with the library plate. The arrangement of the tightening screws was changed, as shown in Fig. 2a. After these modifications to the reactor, the temperature variation across the library improved, and the library could be heated reliably up to 750 °C. The reactor cross-section is shown in Fig. 2. The library plate temperature was set to 600 °C for each measurement. Reaching 600 °C at the library surface took about 1 h, and stabilizing the library plate temperature took another 2 h.

Because of the open construction of the reactor (see Fig. 2), oxygen and moisture from the ambient air cannot be avoided completely. However, during the reaction of each hole, the amount of air from the atmosphere was close to zero between the sampling needle and the sample surface, as determined by a micro-gas chromatograph. Avoiding oxygen was essential to reduce the risk of unexpected oxidation reactions. The reactant gas, a certified calibration gas mixture composed of 52.8 vol% CH_4 and 47.2 vol% CO_2 (CH_4/CO_2 ratio, 1.12), was used without further purification. The flow rate of this gas mixture was always set to 10 ml min^{-1}. The gas composition of products was analysed by a micro-gas chromatograph (model CP 4900;

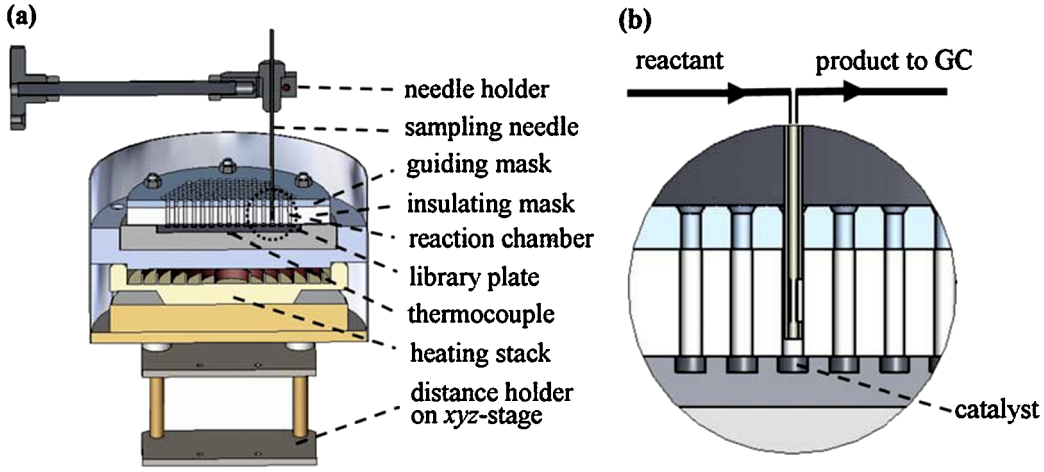

Fig. 2. (a) Cross-section of the assembled reactor and (b) magnification of reaction chambers (dotted-circle in (a)).

Varian) equipped with a thermal conductivity detector. Two packed columns, Porapak Q and molecular sieve 5A columns, were used in parallel to separate CH_4, CO_2 and H_2, CH_4, CO. The high-throughput experiments were controlled by TestRig software [20].

In a standard experiment, it took about 120 s (100 s inside the hole for reaction, 10 s outside the hole for waiting, and another 10 s for xyz-stage moving) to evaluate the catalytic activity for each material by a single GC measurement. Therefore, the initial activity test of 207 catalysts took approximately 7 h. The same high-throughput system was used for the stability test of the components. To assess the stability of each catalyst, the sampling needle was kept inside the hole of each well for 800 s with five GC runs or for 3500 s with 22 GC runs. The activity of each well is represented relative to the maximum activity of the reference catalyst. Although the stability tests take a long time, the experiment is completely automated and does not need much supervision. The rapid initial activity test can have false positives (i.e., rapidly deactivating materials) and false negatives (i.e., materials that activate slowly). Both negatives can be eliminated by the stability test. To enable comparisons of sample stability, the deactivation rate (h^{-1}) of each sample in the high-throughput experiment was defined as [(1 − (the activity at last measurement)/(the maximum activity))/(time-on-stream between a maximum and a last point (h))]. If the relative activity of a sample increased continuously during the measurement, then the deactivation rate was expressed as zero.

2.4. Conventional catalyst syntheses

The procedure of method 3 in high-throughput synthesis was followed for the 50-times-larger scale in a conventional catalyst synthesis. The preparation of $Al_{N5}Ni_{10}Ce_{85}$, for example, was carried out as follows. The complexing agent (4-hydroxy-4-methyl-pentanone, 3.7 ml, 30 mmol) was placed in a 100-ml glass beaker. Then 1 M $Ce(NO_3)_3{\cdot}6H_2O$ solution in methanol (8.5 ml, 8.5 mmol), 1 M $Ni(NO_3)_2{\cdot}6H_2O$ solution in methanol (1.0 ml, 1 mmol), and 1 M $Al(NO_3)_3{\cdot}9H_2O$ solution in methanol (0.5 ml, 0.5 mmol) were added, and the solution was magnetically stirred for 30 min. Propionic acid (15.0 μl, 0.2 mmol) was added dropwise under continuous stirring. The solution was stirred for another 3 h while covered with parafilm, to obtain a homogeneous solution. After the parafilm was removed, the solution was transferred to a wide, shallow beaker and dried for 5 days at 40 °C for gelation. Then it was carefully calcined in an oven at 65 °C for 5 h (at a heating rate of 0.2 °C min^{-1}) and at 250 °C for 5 h (at a heating rate of 0.2 °C min^{-1}). The catalyst powder obtained was ball-milled for 30 min, then recalcined in an oven, heated to 700 °C at a rate of 2 °C min^{-1}, and kept there for 2 h. For comparison, the 10 mol% Ni catalyst supported on commercial γ-Al_2O_3 (Johnson Matthey; $S_{BET} = 255\ m^2\ g^{-1}$), referred to as Ni/$Al_2O_3$, was prepared by wet impregnation.

2.5. Conventional testing of catalysts

Conventional catalytic studies were carried out in a gas-phase quartz tubular flow reactor (7 mm i.d., 400 mm long) at atmospheric pressure. Typically, 100 mg of sample in fine-powder form (25–50 μm) was placed in the center of the reactor and held by quartz wool plugs. The reactor tube was heated inside an electric furnace. A quartz tube-sheathed K-type thermocouple was placed at the top of the catalyst bed to monitor the reaction temperature. The reactant gas (52.8 vol% CH_4 and 47.2 vol% CO_2), diluted with argon, was used without further purification. The typical in situ reduction step was excluded, because the focus was on autoreduction catalysts. The following experimental conditions were used for a typical run. The catalyst was oxidized in situ at 600 °C for 2 h in flowing air (50 ml min^{-1}) under similar conditions as for the high-throughput experiment. After purging with Ar (50 ml min^{-1}) for 30 min, the gas flow was switched to an upstream reactant gas mixture ($CH_4/CO_2/Ar = 16.9/15.1/68$; total flow, 65 ml min^{-1}). After switching, the catalyst bed temperature of the active catalyst was decreased for a short time due to a large endothermic heat change. The gas composition of products was analysed by gas sensors (20 vol% CH_4, 25 vol% CO_2, and 10 vol% CO; GfG-mbH) and a micro-gas chromatograph (model CP 4900; Varian). Each sample was tested for 10 h

with a 60 × GC measurement run. Blank reaction tests without catalyst were carried out to confirm that the reactor and thermocouple itself were not catalytically active. In the conventional experiments, the deactivation rate (h^{-1}) for each catalyst was defined as [(1 − (the activity at last measurement)/(the maximum activity))/(time-on-stream between a maximum and a last point (h))].

2.6. Catalyst characterization

The chemical composition of each catalyst in the libraries was analysed by X-ray fluorescence (XRF) spectroscopy (EAGLE II μ-Probe; EDAX) with Rh-K_α radiation. The X-ray beam was sequentially focused to a spot size of 300 μm on each sample surface of a library.

Total BET surface areas were measured with a nitrogen adsorption apparatus (Sorptomatic 1990, Carlo Erba) at the temperature of liquid nitrogen. The samples were outgassed overnight under vacuum at 200 °C before adsorption.

Temperature-programmed oxidation (TPO) was done by thermogravimetric analysis (TGA) using a Shimadzu TGA-50 thermogravimetric analyser. After 10 h of reaction time, the catalyst sample was cooled to room temperature in a flow of Ar and then transferred to the TGA apparatus. About 50 mg of sample was loaded in a sample pan. The weight change of the catalyst was recorded in a flow of air (15 ml min^{-1}) as temperature was increased from room temperature to 900 °C at a rate of 15 °C min^{-1}.

3. Results and discussion

3.1. High-throughput experiments (generations 1 and 2)

The chemical composition of each catalyst in a library was verified by XRF. The concept of evolution (i.e., variation and selection) was applied for the library design. Variation was obtained by doping and composition spread. Catalyst activity and stability, determined by the amount of CO produced and its deactivation rate, respectively, were chosen for selection. Hit samples, the most active catalysts of one generation, were used as base materials for the catalysts studied in the following generation. Table 1 summarizes the sample composition, preparation method, time on stream, sample number, and active sample of libraries sorted by generation.

Our search for new catalysts began with the systematic doping of $Zr_{20}Al_{80}$, which is known to exhibit extraordinarily high thermal stability [26]. An $E_xZr_{20}Al_{80-x}$ ($x = 1, 5, 10$) library with 177 samples of 59 different dopants (E) was tested. Among these, only precious metal including mixed oxides showed relatively good activity, which decreased in the following order: Rh > Ru > Pt > Pd > Ir ($x = 1$), Rh > Ru > Pd > Ir > Pt ($x = 5$) and Rh > Pd ≈ Pt > Ir > Ru ($x = 10$). This can be explained by the facile reducibility of noble metals and the exceptional catalytic properties of these metals in their metallic state [27]. Low loading (1 mol%) was sufficient for effective performance in the case of Rh and Ru. Fig. 3 describes the relative activity (%) for the $E_xZr_{20}Al_{80-x}$ ($x = 1, 5, 10$) library, presented relative to the activity of $Rh_1Zr_{20}Al_{79}$, the

Table 1
Sample composition, preparation method, time-on-stream, sample number, and active sample of libraries prepared in this study[a]

Generation	Sample composition	Method	Time-on-stream (s)	Sample number	Active sample
1	$E_xZr_{20}Al_{80-x}$[b]	1	100	59 × 3	$(Rh, Ru, Pt, Pd, Ir)_xZr_{20}Al_{80-x}$
	M_3N_{97}[c]	1	100	55 × 6	None
	M_3P_{97}[d]	2	100	55 × 3	V_3Ni_{97}
	M_3Q_{97}[e]	3	100	55 × 5	Ni_3Ce_{97}
	Previous libraries[f]	–	100	≈4000	Rh, Ru, Pt, Pd and Ir containing catalysts
	V_3Ni_{97}, Ni_3Ce_{97}	2, 3	800	2	Ni_3Ce_{97}
2	M_3Ce_{97}	3	800	55	Ni_3Ce_{97}
	$Ni_{10}M_{90}$	3	800	55	$Ni_{10}Ce_{90}$
3	$M_{15}Ni_{10}Ce_{75}$	3	800	54	$(Al_N, Al_A, Si, Ta, Zr_N, Zr_A)_{15}Ni_{10}Ce_{75}$ and $(Cd, Rb, Sc, Se)_{15}Ni_{10}Ce_{75}$
		3	3500	10	$(Al_N, Al_A, Si, Ta, Zr_N, Zr_A)_{15}Ni_{10}Ce_{75}$
4	$R_yNi_{10}Ce_{90-y}$[g]	3	800	6 × 4	$(Al_{N5}, Al_{N15}, Al_{A5}, Al_{A15}, Al_{A45}, Si_5, Si_{15}, Si_{45}, Si_{75}, Ta_{15}, Zr_{N5}, Zr_{N15}, Zr_{N75}, Zr_{A5}, Zr_{A15})Ni_{10}Ce_{90-y}$ and $(Al_{A75}, Zr_{A45}, Zr_{A75})Ni_{10}Ce_{90-y}$
		3	3500	18	$(Al_{N5}, Al_{N15}, Al_{A15}, Zr_{N15}, Zr_{A5}, Zr_{A15})Ni_{10}Ce_{90-y}$

[a] Operating conditions: $T = 600$ °C; $P = 1$ bar; total flow: 10 ml min^{-1} ($CH_4/CO_2 = 1.12$).
[b] E = Ag, Al_N, Al_A, Au, B, Ba, Bi, Ca, Cd, Ce, Co, Cr, Cs, Cu, Dy, Er, Eu, Fe, Ga, Gd, Ge, Hf, Ho, In, Ir, K, La, Li, Lu, Mg, Mn, Mo, Na, Nb, Nd, Ni, Pb, Pd, Pr, Pt, Rb, Re, Rh, Ru, Sb, Sc, Se, Si, Sm, Sn, Sr, Ta, Tb, Te, Ti, Tm, V, W, Y, Yb, Zn, Zr_N, Zr_A. $x = 1, 5, 10$.
[c] M = E—Au, Ir, Pd, Pt, Re, Rh, Ru. N = Cu, Fe, Nb, Sn, Ta, V.
[d] P = Co, Mn, Ni.
[e] Q = Ce, Cr, Ga, In, Zn.
[f] See Table 2.
[g] R = Al_N, Al_A, Si, Ta, Zr_N, Zr_A. $y = 5, 15, 45, 75$.

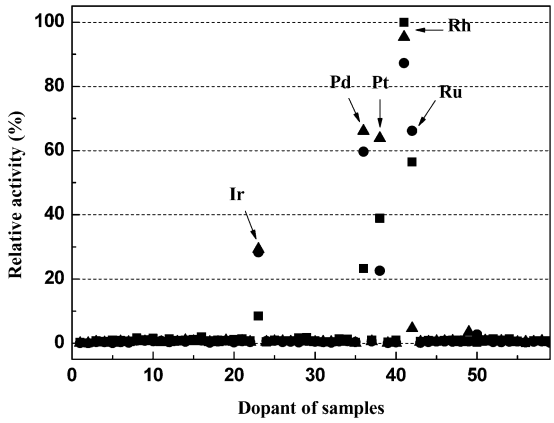

Fig. 3. Relative activity (%) of the $E_xZr_{20}Al_{80-x}$ ($x = 1, 5, 10$) library, normalized to the activity of $Rh_1Zr_{20}Al_{79}$ (most active, reference): $x =$ (■) 1, (●) 5, (▲) 10 mol%. Operating conditions: $T = 600\,^{\circ}C$; $P = 1$ bar; total flow: 10 ml min^{-1} ($CH_4/CO_2 = 1.12$).

Table 2
Composition of mixed oxides on the selected prefabricated libraries studied during the primary screening[a]

Binary and ternary mixed oxide
$(L_1)_x(L_2)_y$ (L = V, Fe, Mo, Cr, Ta, Nb, Mn, Sb, Bi)
$(L_1)_x(L_2)_y(L_3)_z$ (L = V, Fe, Mo, Cr, Ta, Nb, Mn, Sb, Bi)
$Nb_xTa_yTi_z$
Doped Sb oxides
$(L_1)_x(L_2)_ySb_{90}$ (L = Bi, Mo, Nb, Te, Zr, Ta, V, Cr, Mn)
$(L_1)_x(L_2)_ySb_{90}$ (L = Fe, Sn, Cu, Ni, Ce, Ti, Al, Co, La)
Pt containing mixed oxides
$Pt_3(L_1)_x(L_2)_y$ (L = Ti, Ta, V, Al, Zr, Ni, Mn, W, Si, Co, Nb, Fe, Ge, Sn, Mo, Te, Bi)
$Pt_3(L_1)_x(L_2)_y(L_3)_z$ (L = Zr, Al, Ni, Mn, Nb)
$Pt_3(L_1)_x(L_2)_y(L_3)_z(L_4)_t$ (L = Ti, W, Nb, Ta)
Pd containing mixed oxides
$Pd_{0.5}(L_1)_x(L_2)_y$ (L = W, Cr, Nb, Mn, Fe, Ti, Al, Zr, Co, Zn, Ni, Cu, Sn, Ge, Si, Te)
$Pd_{0.5}(L_1)_x(L_2)_y(L_3)_z$ (L = Si, Co, W, Fe, Cu, Cr, Ti)

[a] Operating conditions: $T = 600\,^{\circ}C$; $P = 1$ bar; total flow: 10 ml min^{-1} ($CH_4/CO_2 = 1.12$).

best catalyst in this library. Despite controversy in the literature about the most suitable metal, Rh was always observed to be the most active and stable element in the CO_2 reforming of methane under our reaction conditions [5]. Precious metal-containing catalysts are effective and usually not dependent on prereduction steps. On the other hand, Ni/Al_2O_3 exhibited little CO formation in the initial activity test and even in the stability test over 3500 s. The catalytic activity of this catalyst appears to be highly dependent on the prereduction. $Rh_1Zr_{20}Al_{79}$, the most active catalyst on the $E_xZr_{20}Al_{80-x}$ library was prepared several times by high-throughput synthesis and was used as a reference catalyst on all libraries during generations 1 and 2. Twenty additional libraries available in our research group with almost 4000 samples that had been prepared for other studies were assessed; here also, only precious metal-containing mixed oxides showed effective catalytic activity. Table 2 summarizes the catalysts on the libraries screened unsuccessfully for CO_2 reforming of methane during the primary screening phase of the project.

Because we focused on nonprecious metal catalysts in the present study, we prepared and examined 14 different nonprecious metal (Ce, Co, Cr, Cu, Fe, Ga, In, Mn, Nb, Ni, Sn, Ta, V, and Zn)-based mixed oxides with 55 dopants of 3%. Only a few of these, such as Ni_3Ce_{97} and V_3Ni_{97}, were effective, with activities of 32.5 and 52.5%, respectively, relative to the reference $Rh_1Zr_{20}Al_{79}$. Stability tests of these two catalysts were performed for 800 s. The relative activity of V_3Ni_{97} decreased rapidly from 54.8 to 46.3% (maximum 71.0% at the second run) with a deactivation rate of 2.09 h^{-1}. In contrast, Ni_3Ce_{97} showed good stability with a relative activity of 32.5–32.9% (maximum 33.9 % at the second run). The deactivation rate of Ni_3Ce_{97} was 0.18 h^{-1}. Therefore, Ni_3Ce_{97} was selected for the next generation. In the first generation, more than 5000 mixed oxides were tested, and Ni_3Ce_{97} exhibited the best activity and stability among all of the nonprecious metal catalysts with no prereduction step.

In the second generation, the mixed oxides M_3Ce_{97} and $Ni_{10}M_{90}$ were prepared with 55 different elements M and examined for 800 s to verify the activity of other ceria-based or nickel-including mixed oxides. However, only Ni_3Ce_{97} and $Ni_{10}Ce_{90}$ were significantly active, with relative activities of 32.5 and 93.9%, respectively. $Ni_{10}Ce_{90}$ revealed an effective stability, with relative activity of 93.9–95.1% (maximum 96.4% at the second run). The deactivation rate of $Ni_{10}Ce_{90}$ was 0.08 h^{-1}. Both nickel and ceria were selected as essential elements for the CO_2 reforming of methane with no prereduction step. $Ni_{10}Ce_{90}$ was selected as a hit sample for the subsequent generation due to higher activity and stability.

3.2. Conventional testing (after generations 1 and 2)

After the high-throughput testing of generations 1 and 2, the properties of the best materials needed to be confirmed in a conventional study. $Ni_{10}Ce_{90}$ and Ni/Al_2O_3 were synthesized by method 3 and a simple wet impregnation method, respectively, in a conventional manner. Table 3 shows that $Ni_{10}Ce_{90}$ has a low surface area and Ni/Al_2O_3 has a relatively high surface area, due to the inherent characteristic of each support. Equilibrium conversions of CH_4 and CO_2, calculated by the equiTherm software [28], were 53.1 and 69.4%, respectively, with a H_2/CO ratio of 0.85 at 600 °C. Only at 800 °C did the equilibrium conversions of CH_4 and CO_2 finally reach almost total consumption (87.8 and 99.1%, respectively) with a H_2/CO ratio of 1.

Conventional test results of both catalysts are shown in Fig. 4. $Ni_{10}Ce_{90}$ demonstrated high initial activity (32.3% of CH_4 conversion and 48.7% of CO_2 conversion) with no prereduction. This catalyst revealed rapid deactivation within 30 min, and much less significant deactivation thereafter. In contrast, in Ni/Al_2O_3 activity did not start to increase until after almost 80 min, and catalytic activity stabilized only after about 240 min (long induction period). These findings indicate that Ni/Al_2O_3 should be prereduced to avoid the long induction period. After the activity of Ni/Al_2O_3 stabilized with 30.1% of CH_4 conversion and 37.7% of CO_2 conversion, the conversion of CO_2 slowly decreased while CH_4 consumption slowly

Table 3
Physical property, TGA and results of conventional tests of selected catalysts

Generation	Catalyst	S_{BET}[a] ($m^2\ g^{-1}$)	Conventional testing[b]		TGA[c]
			Max. relative activity (%)	Deactivation rate (h^{-1})	coke ($g_C\ g_{cat}^{-1}$) ($wt\%\ h^{-1}$)
1–2	$Ni_{10}Ce_{90}$	36.9	100.00	0.0181	0.08
	Ni/Al_2O_3	205.9	83.47	–	2.28
3–4	$Al_{N5}Ni_{10}Ce_{85}$	39.6	94.22	0.0138	0.03
	$Al_{N15}Ni_{10}Ce_{75}$	61.9	87.93	0.0109	0.19
	$Al_{A15}Ni_{10}Ce_{75}$	54.1	112.13	0.0093	0.38
	$Zr_{N15}Ni_{10}Ce_{75}$	39.2	106.29	0.0134	0.09
	$Zr_{A5}Ni_{10}Ce_{85}$	45.1	111.04	0.0125	0.24
	$Zr_{A15}Ni_{10}Ce_{75}$	47.4	106.97	0.0109	0.38

[a] Measured after calcination in air at 700 °C for 2 h.
[b] Operating conditions: $T = 600\,°C$; $P = 1$ bar; total flow: 65 ml min^{-1} ($CH_4/CO_2/Ar = 16.9/15.1/68$); catalyst weight: 0.100 g; time-on-stream: 10 h.
[c] Operating conditions: catalyst weight, ≈0.050 g; T increasing rate: 15 °C min^{-1}; air total flow: 15 ml min^{-1}.

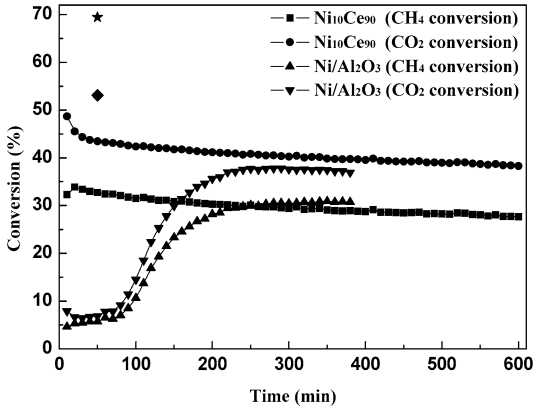

Fig. 4. Time dependence of the catalytic activity and stability of $Ni_{10}Ce_{90}$ and Ni/Al_2O_3 in conventional test: CH_4 conversion (■) and CO_2 conversion (●) of $Ni_{10}Ce_{90}$; CH_4 conversion (▲) and CO_2 conversion (▼) of Ni/Al_2O_3; calculated equilibrium conversion of CH_4 (◆) and CO_2 (★). Operating conditions: $T = 600\,°C$; $P = 1$ bar; total flow: 65 ml min^{-1} ($CH_4/CO_2/Ar = 16.9/15.1/68$); catalyst weight: 0.100 g.

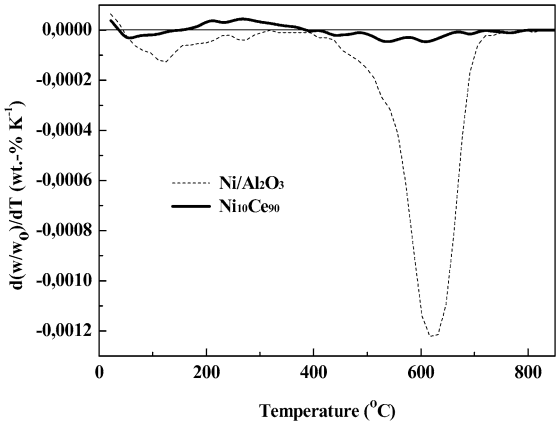

Fig. 5. d–TGA profile of used $Ni_{10}Ce_{90}$ (—) (after 600 min reaction time) and used Ni/Al_2O_3 (···) (after 380 min reaction time). Operating conditions: catalyst weight: ≈0.050 g; T increasing rate: 15 °C min^{-1}; air total flow: 15 ml min^{-1}.

increased, leading to reactor plugging after 380 min. These results confirm that the growth of carbon formation is dominated by methane decomposition. The gas hourly space velocities (GHSVs) of these catalysts are of interest. The GHSVs of $Ni_{10}Ce_{90}$ and Ni/Al_2O_3 were 139,000 (h^{-1}) and 36,000 (h^{-1}), respectively. Considering the surface area and GHSV of each catalyst, the active site of $Ni_{10}Ce_{90}$ seems to be more efficient than that of Ni/Al_2O_3.

The conversions of both catalysts do not reach thermodynamic equilibrium (see Fig. 4) for two reasons, space velocity and deactivation. Testing 200 mg of $Ni_{10}Ce_{90}$ (GHSV 70,000 h^{-1}) and 400 mg of $Ni_{10}Ce_{90}$ (GHSV 35,000 h^{-1}) under identical conditions demonstrated that only the latter reached close to thermodynamic equilibrium with 49.3% CH_4 conversion and 62.7% CO_2. For 100 mg of $Ni_{10}Ce_{90}$, the GHSV of 139,000 (h^{-1}) is too high to reach thermodynamic equilibrium. Catalyst deactivation within the first 10 min also often contributes to this partial conversion. However, because reaching thermodynamic equilibrium would not reveal any differences in catalytic performance, these reaction conditions were chosen deliberately.

The results of the conventional study within 60 min of reaction time are in accordance with those of the high-throughput screening for 3500 s. Initial high activity followed by rapid deactivation of $Ni_{10}Ce_{90}$ and low activity of Ni/Al_2O_3 were observed in both experiments. The good agreement between the combinatorial results and the results obtained under conventional reaction conditions confirms that the development of catalysts for CO_2 reforming of methane can be carried out reliably using a simple high-throughput method.

Carbon (coke) deposition is thermodynamically favoured at our experimental conditions of low temperature (600 °C) and a high CH_4/CO_2 ratio of 1.12. It has been reported that at low CH_4/CO_2 ratios (<1) and high-temperature (>800 °C), carbon formation is significantly reduced [4–6,29].

The weight change during TPO of $Ni_{10}Ce_{90}$ used for 600 min and Ni/Al_2O_3 for 380 min was measured by TGA. The weights of sample were normalized with respect to the initial sample weight and then differentiated with respect to temperature for d–TGA pattern. The d–TGA profiles are shown in Fig. 5. Two main peaks appeared for the used Ni/Al_2O_3. The first peak, observed between 50 and 320 °C with a weight loss of 0.22 wt% (h^{-1}), can be assigned to water desorbing from the

catalyst surface. The second weight loss occurred in the temperature range of 400–800 °C with a weight change of 2.28 wt% (h^{-1}), and can be assigned to oxidation of deposited carbon. The d–TGA pattern of the used $Ni_{10}Ce_{90}$ showed three different peaks. The first peak, at 40–155 °C with a weight loss of 0.01 wt% (h^{-1}), can be assigned to desorption of water. The third peak, at 400–800 °C with a weight loss of 0.08 wt% (h^{-1}), can be assigned to the oxidation of carbon deposition as in the case of Ni/Al_2O_3. The second peak, representing a weight gain rather than a weight loss, appeared at 160–385 °C with a weight change of 0.06 wt% (h^{-1}). This surprising behaviour is attributed to oxygen chemisorption into the oxygen vacancies of cerium oxide generated during the reaction. However, determining the amount of chemisorbed oxygen was difficult, because the first and second peaks overlapped. The weight gain peak was also observed in d–TGA results on fresh $Ni_{10}Ce_{90}$ reduced by hydrogen, but it was not detected in d–TGA results on fresh $Ni_{10}Ce_{90}$ calcined in ambient air. A study of three-way catalysts found a similar weight recovery when pulses of hydrogen were followed by pulses of oxygen on cerium oxide [30].

Two advantages of $Ni_{10}Ce_{90}$ over Ni/Al_2O_3 can be discerned from the conventional testing and TGA findings. $Ni_{10}Ce_{90}$ activates rapidly with no prereduction and has a much higher resistance to coking. These positive properties seem to result from the high oxygen storage and release capacity (OSC) of cerium oxide, leading to highly mobile oxygen species during the reaction. A more detailed investigation to elucidate these mechanisms is currently underway.

3.3. High-throughput experiments (generations 3 and 4)

A major drawback of the $Ni_{10}Ce_{90}$ is deactivation, which can be related to three different phenomena: (1) sintering of the Ni particles, leading to a loss of active sites; (2) carbon deposition, resulting in a blocking of active sites; and (3) decreased cerium oxide surface area, leading to a deficiency in OSC. Reason (2), carbon deposition, seems negligible because of the small amount of total carbon (0.08 wt% h^{-1}) shown in Fig. 5. Therefore, the other two reasons are more likely to be relevant for the deactivation of $Ni_{10}Ce_{90}$. It is well known that a pure CeO_2 surface is not very stable at high temperatures under reducing conditions, leading to collapse of surface area and significant deactivation of the redox couple [30–32]. Previous studies have evaluated mixed oxides of ceria (e.g., CeO_2–Al_2O_3, CeO_2–SiO_2, CeO_2–La_2O_3, CeO_2–HfO_2, and CeO_2–ZrO_2) with the aim of increasing thermal stability and preventing the decline of OSC [30–32].

A similar approach was chosen for the present study. To promote the thermal stability, carbon-free operation, and OSC of $Ni_{10}Ce_{90}$, a third oxide of 15 mol% (54 different elements) was introduced using the sol–gel process. An $M_{15}Ni_{10}Ce_{75}$ library was prepared and tested (generation 3). $Ni_{10}Ce_{90}$ was used as reference catalyst during generations 3 and 4. Among the 54 samples of the $M_{15}Ni_{10}Ce_{75}$ library, only a few catalysts, including $(Al_N, Al_A, Si, Ta, Zr_N, Zr_A)_{15}Ni_{10}Ce_{75}$, showed comparable activity and better stability for 800 s relative to $Ni_{10}Ce_{90}$. To reduce false negatives due to slowly activated

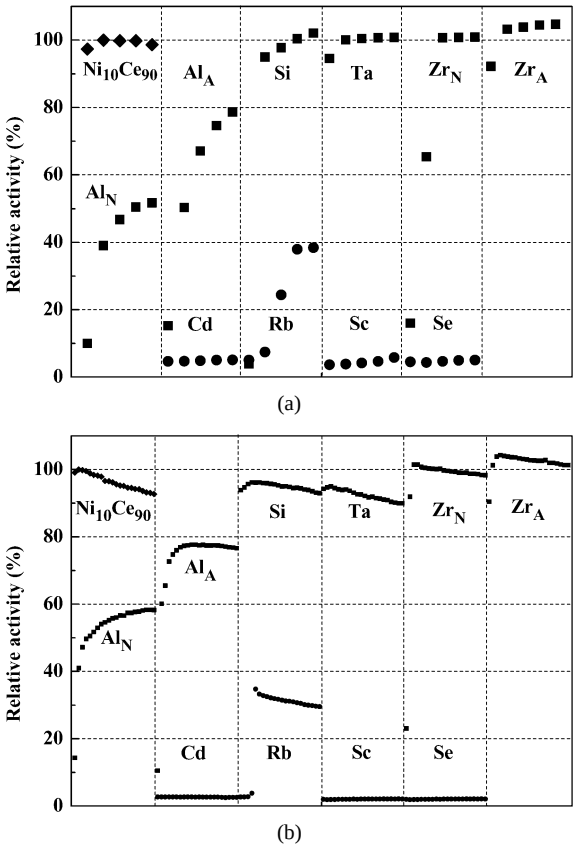

Fig. 6. Time dependence of the catalytic activity (%) of selected materials on the $M_{15}Ni_{10}Ce_{75}$ library relative to the reference catalyst $Ni_{10}Ce_{90}$ in high-throughput tests during (a) 800 and (b) 3500 s: (◆) $Ni_{10}Ce$; (■) $(Al_N, Al_A, Si, Ta, Zr_N, Zr_A)_{15}Ni_{10}Ce_{75}$; (●) $(Cd, Rb, Sc, Se)_{15}Ni_{10}Ce_{75}$. Operating conditions: $T = 600$ °C; $P = 1$ bar; total flow: 10 ml min^{-1} ($CH_4/CO_2 = 1.12$).

candidates, which could originate from relatively short time on stream, $(Cd, Rb, Sc, Se)_{15}Ni_{10}Ce_{75}$ were also chosen, due to their low but increasing activity with time (see Fig. 6). Fig. 6a depicts the relative activities (%) of $Ni_{10}Ce_{90}$ and 10 candidates after 800 s of reaction time. The deactivation rate was 0.08 h^{-1} for $Ni_{10}Ce_{90}$ and 0 for the 10 candidates. These ten samples and $Ni_{10}Ce_{90}$ were checked again for 3500 s. The relative activities (%) of $Ni_{10}Ce_{90}$ and the 10 candidates for 3500 s are shown in Fig. 6b. $(Cd, Rb, Sc, Se)_{15}Ni_{10}Ce_{75}$ revealed only poor activity during the measurement; therefore, these four catalysts were excluded in the next generation of catalysts. Comparable activity and a reduced deactivation rate were observed for $(Al_N, Al_A, Si, Ta, Zr_N, Zr_A)_{15}Ni_{10}Ce_{75}$ relative to $Ni_{10}Ce_{90}$. Deactivation rates of 0.08 h^{-1} for $Ni_{10}Ce_{90}$ and 0, 0.03, 0.04, 0.06, 0.04, and 0.04 h^{-1} for $(Al_N, Al_A, Si, Ta, Zr_N, Zr_A)_{15}Ni_{10}Ce_{75}$ were observed. These catalysts are the hits of generation 3, selected for further improvements.

In generation 4, the amount of third element was varied stepwise in 5, 15, 45, and 75 mol% for selected catalysts of generation 3. Fig. 7a describes the relative activities (%) of $Ni_{10}Ce_{90}$ and $(Al_N, Al_A, Si, Ta, Zr_N, Zr_A)_yNi_{10}Ce_{90-y}$ ($y = 5$, 15, 45, 75) mixed oxides after 800 s of reaction time. Some of these, including (Al_{N5}, Al_{N15}, Al_{A5}, Al_{A15}, Al_{A45}, Si_5, Si_{15}, Si_{45}, Si_{75}, Ta_{15}, Zr_{N5}, Zr_{N15}, Zr_{N75}, Zr_{A5},

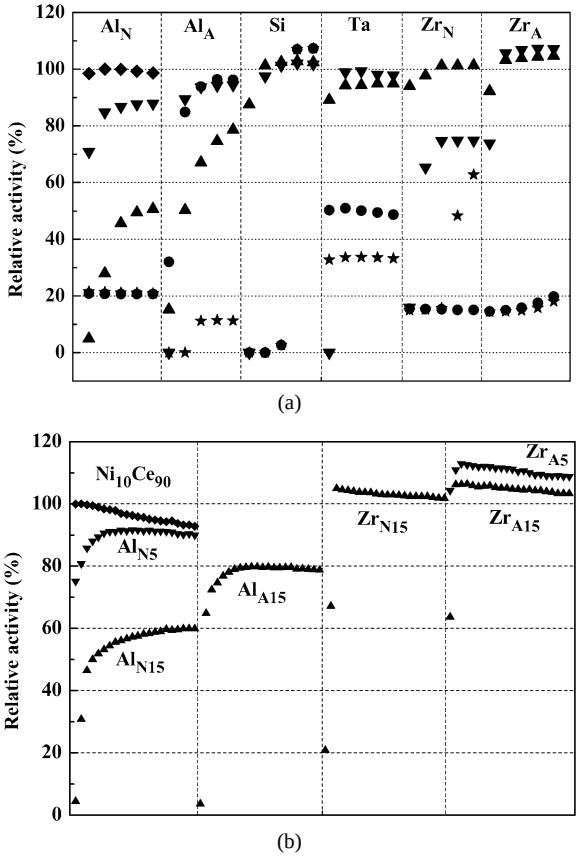

Fig. 7. Time dependence of the catalytic activity (%) of selected materials of the (Al_N, Al_A, Si, Ta, Zr_N, Zr_A)$_y$$Ni_{10}Ce_{90-y}$ (y = 5, 15, 45, 75) library relative to the reference catalyst $Ni_{10}Ce_{90}$ in high-throughput tests during (a) 800 and (b) 3500 s: (◆) $Ni_{10}Ce_{90}$; y = (▼) 5, (▲) 15, (●) 45, (★) 75 mol%. Operating conditions: T = 600 °C; P = 1 bar; total flow: 10 ml min^{-1} (CH_4/CO_2 = 1.12).

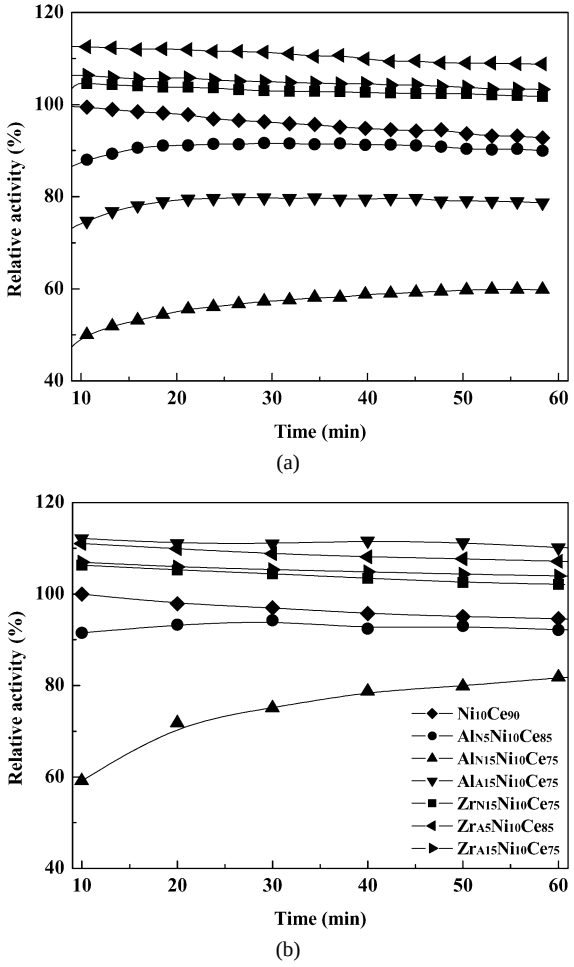

Fig. 8. Time dependence of the catalytic activity (%) of the best catalysts relative to the reference $Ni_{10}Ce_{90}$ in (a) high-throughput testing during 3500 s and (b) conventional tests within the first 3600 s: (◆) $Ni_{10}Ce_{90}$; (●) $Al_{N5}Ni_{10}Ce_{85}$; (▲) $Al_{N15}Ni_{10}Ce_{75}$; (▼) $Al_{A15}Ni_{10}Ce_{75}$; (■) Zr_{N15}-$Ni_{10}Ce_{75}$; (◄) $Zr_{A5}Ni_{10}Ce_{85}$; (►) $Zr_{A15}Ni_{10}Ce_{75}$.

$Zr_{A15})Ni_{10}Ce_{90-y}$, exhibited similar activities and lower deactivation rates compared with $Ni_{10}Ce_{90}$. A zero deactivation rate was found for all of these materials except $Ni_{10}Ce_{90}$ (0.08 h^{-1}), $Al_{A45}Ni_{10}Ce_{45}$ (0.01 h^{-1}), and $Si_5Ni_{10}Ce_{85}$ (0.01 h^{-1}). (Al_{A75}, Zr_{A45}, Zr_{A75})$Ni_{10}Ce_{90-y}$ were also selected because of their zero deactivation rates despite low relative activities. The selected samples and $Ni_{10}Ce_{90}$ were retested for another 3500 s. Among these samples, (Al_{N5}, Al_{N15}, Al_{A15}, Zr_{N15}, Zr_{A5}, Zr_{A15})$Ni_{10}Ce_{90-y}$ had activities comparable to the activity of $Ni_{10}Ce_{90}$ and a deactivation rate of <0.04 h^{-1}, as shown in Fig. 7b. The deactivation rates of these catalysts were 0.08 h^{-1} for $Ni_{10}Ce_{90}$ and 0.04, 0, 0.03, 0.03, 0.04, and 0.03 h^{-1} for (Al_{N5}, Al_{N15}, Al_{A15}, Zr_{N15}, Zr_{A5}, Zr_{A15})$Ni_{10}Ce_{90-y}$, respectively, which were selected as hit catalysts from generation 4. The high-throughput optimisation was terminated at this stage.

3.4. Conventional testing (after generations 3 and 4)

The best catalysts from generation 4 were synthesized and examined by conventional experiments. Table 3 summarizes the physical properties and results of conventional testing and TGA of these selected catalysts. The maximum relative activity (%) was defined as [(the maximum amount of CO produced on a catalyst)/(the maximum amount of CO produced on $Ni_{10}Ce_{90}$)×100] during 10 h of reaction. The maximum activity was observed at the first measurement after 10 min in all catalysts but $Al_{N5}Ni_{10}Ce_{85}$ (30 min) and $Al_{N15}Ni_{10}Ce_{75}$ (210 min). The surface areas of all catalysts were slightly increased relative to that of $Ni_{10}Ce_{90}$, especially those of $Al_{N15}Ni_{10}Ce_{75}$ and $Al_{A15}Ni_{10}Ce_{75}$. Fig. 8 compares high-throughput testing for 3500 s and conventional testing within the first 60 min. The relative activities after the same time on stream were very similar for (Al_{N5}, Zr_{N15}, Zr_{A5}, Zr_{A15})$Ni_{10}Ce_{90-y}$ but increased for $Al_{N15}Ni_{10}Ce_{75}$ and $Al_{A15}Ni_{10}Ce_{75}$. This finding is attributed to the different catalyst loading methods in high-throughput testing and conventional testing. In the high-throughput experiment, the same volume of catalyst powder is filled in library wells, and the same weight is charged in the conventional gas-phase reactor. On BET measurements, $Al_{N15}Ni_{10}Ce_{75}$ and $Al_{A15}Ni_{10}Ce_{75}$ showed much larger surface areas than $Ni_{10}Ce_{90}$, indicating that their lower weight was filled in a library well, which may be the reason for the increased activity in the conventional tests.

The third elements of the catalysts affected the catalytic properties in the following order: (1) maximum activity: Al_{A15} ≈

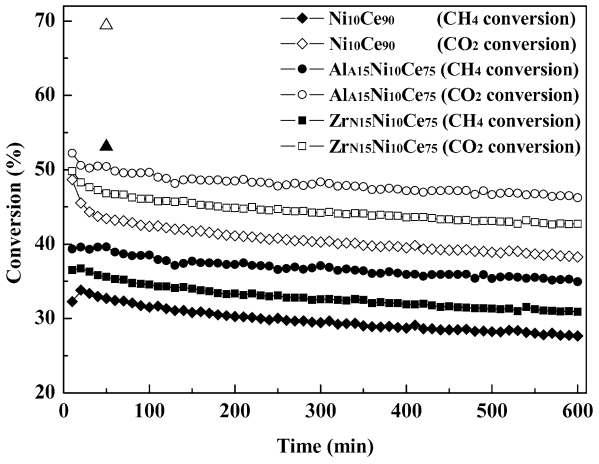

Fig. 9. Time dependence of the catalytic activity of $Al_{A15}Ni_{10}Ce_{75}$ and $Zr_{N15}Ni_{10}Ce_{75}$ relative to $Ni_{10}Ce_{90}$ in conventional tests: CH_4 conversion (◆) and CO_2 conversion (◇) of $Ni_{10}Ce_{90}$; CH_4 conversion (●) and CO_2 conversion (○) of $Al_{A15}Ni_{10}Ce_{75}$; CH_4 conversion (■) and CO_2 conversion (□) of $Zr_{N15}Ni_{10}Ce_{75}$; calculated equilibrium conversion of CH_4 (▲) and CO_2 (△). Operating conditions: $T = 600\,^{\circ}C$; $P = 1$ bar; total flow: 65 ml min^{-1} ($CH_4/CO_2/Ar = 16.9/15.1/68$); catalyst weight: 0.100 g.

$Zr_{A5} > Zr_{A15} \approx Zr_{N15} >$ none $> Al_{N5} > Al_{N15}$; (2) deactivation rate: none $> Al_{N5} > Zr_{N15} > Zr_{A5} > Al_{N15} \approx Zr_{A15} > Al_{A15}$; (3) carbon deposition: $Al_{A15} \approx Zr_{A15} > Zr_{A5} > Al_{N15} > Zr_{N15} \approx$ none $\approx Al_{N5}$. It has been shown that third elements affect the behaviour of catalysts of lower activity (Al_{N5}, Al_{N15}) and higher activity (Al_{A15}, Zr_{A5}, Zr_{A15}, and Zr_{N15}) and increase their stability in comparison with $Ni_{10}Ce_{90}$. Carbon deposition increased slightly in all samples but $Al_{N5}Ni_{10}Ce_{85}$ and $Zr_{N15}Ni_{10}Ce_{75}$.

$Al_{A15}Ni_{10}Ce_{75}$ seems to be a good new catalyst with respect to its activity and stability despite its tendency toward carbon deposition, and $Zr_{N15}Ni_{10}Ce_{75}$ is most attractive because of its high activity and low tendency toward coking despite its deactivation behaviour. Fig. 9 gives an overview of the conventional test results for $Al_{A15}Ni_{10}Ce_{75}$ and $Zr_{N15}Ni_{10}Ce_{75}$ in comparison with $Ni_{10}Ce_{90}$. The origin of the dramatic effects of the third elements on activity, deactivation, and coking of the catalysts in the CO_2 reforming of methane remains to be clarified.

4. Conclusion

The discovery and optimization of new autoreduction catalysts for the CO_2 reforming of methane have been achieved by high-throughput experimentation. The general strategy for this high-throughput experiment involved both the creation of a library of spatially separated catalysts and evaluation of the materials in the library in terms of initial and long-term performance. A simple open-well high-throughput reactor system connected to a micro-gas chromatograph was used to test catalyst activity and stability at 600 °C. As has been confirmed by conventional experiments, the unavoidable oxygen leakage into the open reactor in the high-throughput experiment does not affect the primary screening approach followed here.

During generations 1 and 2, more than 5000 mixed oxides had been tested. Noble metal-containing catalysts revealed high activity, and among non-precious metal catalysts, $Ni_{10}Ce_{90}$ showed the highest activity and stability with no prereduction step. Both Ni and Ce seem to be essential elements in the CO_2 reforming of methane in the absence of catalyst prereduction. Rapid initial activity and high coking resistance of $Ni_{10}Ce_{90}$ were recognized in a conventional gas-phase study and TGA of the $Ni_{10}Ce_{90}$ after generations 1 and 2. In comparison, a conventional Ni/Al_2O_3 required about 240 min to reach stable activity, and strong carbon deposition led to reactor clogging after only 380 min.

In generations 3 and 4, the deactivation behaviour of $Ni_{10}Ce_{90}$, was significantly reduced by doping with third elements. (Al_{N5}, Al_{N15}, Al_{A15}, Zr_{N15}, Zr_{A5}, Zr_{A15})$Ni_{10}Ce_{90-y}$ exhibited comparable activity and strongly reduced deactivation relative to $Ni_{10}Ce_{90}$. In the conventional tests of the best catalysts after generations 3 and 4, a significantly improved performance of the best catalysts, especially $Al_{A15}Ni_{10}Ce_{75}$ and $Zr_{N15}Ni_{10}Ce_{75}$, could be confirmed (discoveries). Despite the high diversity of our primary screening (see Tables 1 and 2), our search converged to elements all known in the field. Our search essentially confirmed the state of the art, and the discovery quality is reduced to the actual combination and composition of the new catalysts. Apparently, the published and unpublished research in this important area is rather comprehensive. Our initial aim of introducing new elements into the field of methane reforming was not fulfilled. The exceptional catalytic activity and stability of the new Ni-catalysts is attributed to the acid catalyzed sol–gel preparation, which is known to provide atomically dispersed mixed oxides (this has not been proven experimentally).

The good reproducibility of the combinatorial results from primary screening in conventional experiments was verified through catalytic measurements during all four catalyst generations. It has been demonstrated that a simple high-throughput technology can be successfully applied to search for new catalyst formulations even in high-temperature reactions, as long as reaction conditions are chosen such that equilibrium is not reached.

Acknowledgments

Financial support was provided by the Deutsche Forschungsgemeinschaft (grant GRK 232). The authors thank R. Richter for constructing the new reactor, H. Höltzen for assisting with product analysis, and R. Nagel for helping with the BET measurements.

References

[1] J. Huang, R.J. Crookes, Fuel 77 (1998) 1793.
[2] J.M. Fox III, Catal. Rev.-Sci. Eng. 35 (1993) 169.
[3] A.T. Ashcroft, A.K. Cheetham, M.L.H. Green, P.D.F. Vernon, Nature 352 (1991) 225.
[4] M.C.J. Bradford, M.A. Vannice, Catal. Rev.-Sci. Eng. 41 (1999) 1.
[5] J.H. Edwards, A.M. Maitra, Fuel Process. Technol. 42 (1995) 269.
[6] S. Wang, G.Q. Lu, G.J. Millar, Energy Fuels 10 (1996) 896.
[7] M.F. Mark, W.F. Maier, J. Catal. 164 (1996) 122.
[8] www.fuelcells.umicore.com/de/downloads/fcprotonics032004.pdf.

[9] J.A.C. Dias, J.M. Assaf, J. Power Sources 139 (2005) 176.
[10] P.H. Matter, D.J. Braden, U.S. Ozkan, J. Catal. 223 (2004) 340.
[11] J. Scheidtmann, P.-A.W. Weiss, W.F. Maier, Appl. Catal. A 222 (2001) 79.
[12] S. Senkan, Angew. Chem. Int. Ed. 40 (2001) 312.
[13] H. Koinuma, I. Takeuchi, Nat. Mater. 3 (2004) 429.
[14] S.I. Woo, K.W. Kim, H.Y. Cho, K.S. Oh, M.K. Jeon, N.H. Tarte, T.S. Kim, A. Mahmood, QSAR Comb. Sci. 24 (1) (2005) 138.
[15] S. Bergh, S. Guan, A. Hagemeyer, C. Lugmair, H. Turner, A.F. Volpe, W.H. Weinberg, G. Mott, Appl. Catal. A 254 (2003) 67.
[16] D. Wolf, O.V. Buyevskaya, M. Baerns, Appl. Catal. A 200 (2000) 63.
[17] J.M. Serra, A. Chica, A. Corma, Appl. Catal. A 239 (2003) 35.
[18] K.-S. Sohn, J.M. Lee, N. Shin, Adv. Mater. 15 (2003) 2081.
[19] M. Orschel, J. Klein, H.-W. Schmidt, W.F. Maier, Angew. Chem. Int. Ed. 38 (1999) 2791.
[20] J. Urschey, P.-A.W. Weiss, J. Scheidtmann, R. Richter, W.F. Maier, Solid State Sci. 5 (2003) 909.
[21] P.-A.W. Weiss, J.W. Saalfrank, J. Scheidtmann, H.-W. Schmidt, W.F. Maier, in: R.A. Potyrailo, E.J. Amis (Eds.), High Throughput Analysis: A Tool for Combinatorial Materials Science, Kluwer Academic/Plenum, New York, 2003, p. 125.
[22] A. Holzwarth, H.-W. Schmidt, W.F. Maier, Angew. Chem. Int. Ed. 37 (1998) 2644.
[23] J.W. Saalfrank, W.F. Maier, Angew. Chem. Int. Ed. 43 (2004) 2028.
[24] T. Wolter, W.F. Maier, in: R.A. Potyrailo, A. Karim, Q. Wang, T. Chikyow (Eds.), MRS-Symposium Proceedings, vol. 804, MRS, Pittsburgh, 2004, p. 283.
[25] J. Scheidtmann, J.W. Saalfrank, W.F. Maier, Stud. Surf. Sci. Catal. 145 (2003) 13.
[26] J. Klein, W.F. Maier, Chem. Mater. 11 (1999) 2584.
[27] K. Tomishige, S. Kanazawa, M. Sato, K. Ikushima, K. Kunimori, Catal. Lett. 84 (2002) 69.
[28] equiTherm, Version 3.02, Scienceware/VCH (1997).
[29] A.M. Gadalla, B. Bower, Chem. Eng. Sci. 43 (1988) 3049.
[30] E. Rocchini, A. Trovarelli, J. Llorca, G.W. Graham, W.H. Weber, M. Maciejewski, A. Baiker, J. Catal. 194 (2000) 461.
[31] A. Trovarelli, Catal. Rev.-Sci. Eng. 38 (1996) 439.
[32] J. Kaŝpar, P. Fornasiero, M. Graziani, Catal. Today 50 (1999) 285.